Theory of Alloy
Evolution & Dynamics

Technical Highlights

Sandia National Laboratories
Livermore, CA

Term of review FY99 – FY2001

Contact:Robert Q. Hwang,
Sandia National Laboratories, Livermore, CA 94551
Telephone: (925) 294-1570
Fax: (925) 294-3231
Email: rqhwang@sandia.gov

Sandia National Laboratories

Technical Highlights

Vibrational stabilization of the θ phase in Al_2Cu

V. Ozolins and C. Wolverton***
**Sandia National Laboratories, California*
***Ford Motor Corp., Dearborn, Michigan*

Publication:

C. Wolverton and V. Ozolins, "Entropically favored ordering: The metallurgy of Al_2Cu revisited", **Physical Review Letters 86**, 5518 (2001).

Motivation:

The Al-Cu system has played a pivotal role in the understanding of precipitation hardening, a process that many is used on many current commercial alloys. Wilm accidentally discovered this phenomenon in an Al-Cu-based alloy in 1911. Guinier and Preston in the 1930s independently observed Cu-rich precipitates in Al-Cu alloys and realized that precipitation is the structural cause of hardening. The famous sequence of precipitates that form upon heat treating Al-Cu is part of nearly every metallurgical textbook. Upon isothermal aging the disordered Al-Cu alloy often gives way first to small disk-shaped clusters of Cu atoms (called "Guinier-Preston zones"), then to a metastable Al_2Cu phase called θ', and finally to the equilibrium Al_2Cu phase, θ. The last transformation is particularly important since a sizable drop in alloy hardness accompanies the transformation to the equilibrium θ phase. Thus, the stability of the θ' phase relative to the equilibrium θ phase is of considerable interest in commercial processing of Al-Cu alloys.

Accomplishment:

Numerous precipitation (and other) experiments have led to a long-standing belief that the energetic ground state of Al_2Cu is the θ phase. State-of-the-art first-principles calculations of the relative stability of θ and θ' lead to the following surprising result: *Although* θ *is the observed stable phase of Al_2Cu, state-of-the-art first-principles calculations predict the T=0 energy of* θ' *to be below that of* θ. This energetic ordering was found consistently for several electronic-structure methods and exchange-correlation functionals, with the most accurate calculation yielding an energy difference of +15 meV/atom. We show that vibrational entropy reverses this energetic preference at T~200 ^{o}C, resolves the apparent discrepancy between theory and experiment, and hence plays a critical (but previously unsuspected) role in the precipitation sequence.

To assess the magnitude of the entropy due to vibrations in Al_2Cu, we used first-principles density functional linear response theory to calculate harmonic phonon dispersion curves of the θ and θ' phases. The calculated phonon densities of states (DOS) of θ and θ' are shown in Fig. 1. It is seen that the phonon DOS of θ has more weight in the low-frequency region between 100 and 200 cm^{-1}. We obtain a remarkably large positive value of the harmonic entropy difference between θ and θ', $\Delta S_{vib}(\theta/\theta')=+0.37\ k_B$/atom, demonstrating that vibrational entropy strongly favors the tetragonal θ phase over the cubic θ', whereas T=0 energetics has the opposite tendency. Using our result for the structural energy difference between θ and θ', we find that θ will be favored over θ' above T_c *~200* ^{o}C. *Thus, the harmonic vibrational entropy reverses the*

relative high-temperature stability of θ and θ', reconciling the observed precipitation sequence with the theoretically calculated structural stabilities in the Al-Cu system.

Significance:

We have showed that vibrational entropy can produce qualitative changes in phase diagrams by changing the stable ordered state and its underlying structure type. Whether this effect is unique to Al_2Cu or whether it has broader implications for the high-temperature structural stability of many low-symmetry intermetallic phases remains to be explored. Our work on the Al-Sc system (see section "Thermodynamic Properties of Al-Sc Alloys") indicates that vibrational stabilization of "strange" low-symmetry phases over highly symmetric phases could be more general than previously suspected.

FIGURE:

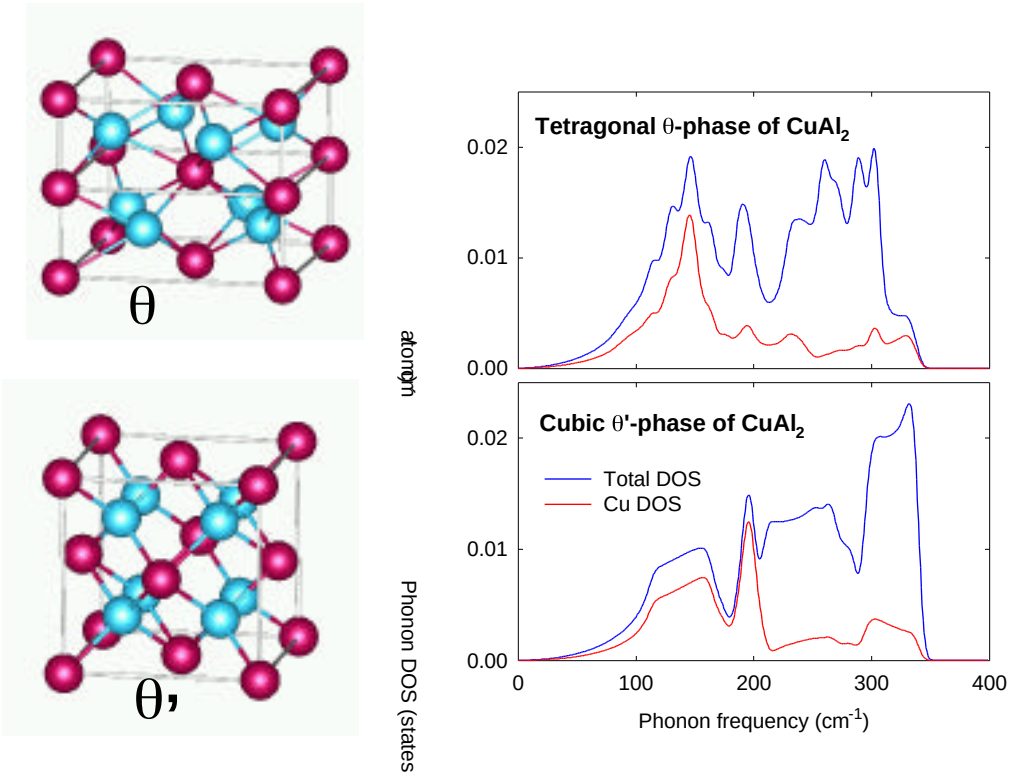

FIG. 1. Structure of Al_2Cu precipitate phases: tetragonal θ phase (top left) and cubic CaF_2-type structure corresponding to unstrained θ' (bottom left). Al atoms are purple and Cu atoms are light blue. The calculated phonon densities of states (DOS) for both phases are shown in the right panel. Vibrational entropy of the tetragonal θ (Al_2Cu) phase is $+0.37k_B$/atom higher due to larger spectral weight at low frequencies, arising from low-frequency optical branches between 100 cm^{-1} and 200 cm^{-1}.

Large Vibrational Effects upon the Phase Diagram of Al-Sc

V. Ozolins and M. Asta***
**Sandia National Laboratories, California*
***Northwestern University, Evanston, Illinois*

Publication:

V. Ozolins and M. Asta, "Large vibrational effects upon calculated Phase Boundaries in Al-Sc", **Physical Review Letters 86**, 448 (2001).

Motivation:

Traditionally, it has been assumed that the *configurational* entropy plays a dominant role in determining phase diagrams of substitutional alloys. However, *non-configurational* entropy (e.g., magnetic, vibrational) can contribute significantly to the thermodynamic properties of alloy phases. In spite of several experimental papers by B. Fultz and collaborators, who find large differences between the vibrational entropies of ordered and disordered alloy phases in such systems as Cu_3Au, Ni_3Al, and Fe_3Al, theoretical indications of a large effect of vibrational entropy upon the calculated phase diagrams are very scarce.

Accomplishment:

In a previous first-principles study of the technologically important Al-Sc system, M. Asta, S. M. Foiles, and A. Quong [Phys. Rev. B **57**, 11265 (1998)] found that the measured solubility limits for Sc in FCC Al are significantly underestimated (as shown by the dotted line in Fig. 1). In particular, at the eutectic temperature of 933 K, measured and calculated solubility limits were found to differ by roughly a factor of 30. It was hypothesized, based upon an analysis of the temperature dependence of the measured solubility limits, that this discrepancy could be attributed to the neglect of non-configurational entropy contributions to the Gibbs free energies of $L1_2$ (Al_3Sc) and of dilute Sc impurities in Al matrix.

Since then, we have incorporated vibrational contributions to the Gibbs free energy in the calculation of the FCC-based Al-rich part of the Al-Sc phase diagram. Using first-principles linear response calculations we find that the ordered Al_3Sc compound has a very large negative vibrational excess entropy, $\Delta S_{vib}(Al_3Sc) = -0.7\, k_B$/atom. In contrast, the Sc impurity in fcc Al is predicted to exhibit a slightly *positive* excess vibrational entropy. We obtain for the difference in excess entropies per Sc atom a value of $\Delta S_{vib}(Sc) - \Delta S_{vib}(Al_3Sc) = +3.3\, k_B$, which gives a 27-fold increase in the calculated solubility of Sc in Al. The solid line in Fig. 1 shows the effect of the harmonic vibrational entropy on the calculated solubility limit. We see that inclusion of vibrational effects dramatically improves the theoretically calculated solvus boundary and brings the calculated and measured data in excellent agreement with each other. Thermal expansion decreases solubility slightly, as shown by the dash-dotted line in Fig. 1.

Significance:

Thus, we found that *vibrational contributions give rise to a factor of 27 increase in the calculated solubility limits for Sc in FCC Al*, ultimately resulting in a very good level of agreement between measurements and calculated results. The present work gives a clear example demonstrating a large effect of vibrational entropy upon calculated phase boundaries in substitutional alloys.

FIGURES:

FIG. 1. Measured (symbols), and first-principles-calculated Al-rich solvus boundaries for Al-Sc alloys. Dotted and dot-dashed lines correspond to calculations with T=0 K energies and T>0 K electronic free energies, respectively, neglecting vibrational effects. Solid and dashed lines are calculated results including vibrational entropy in the harmonic and quasi-harmonic approximations (i.e., including thermal expansion), respectively.

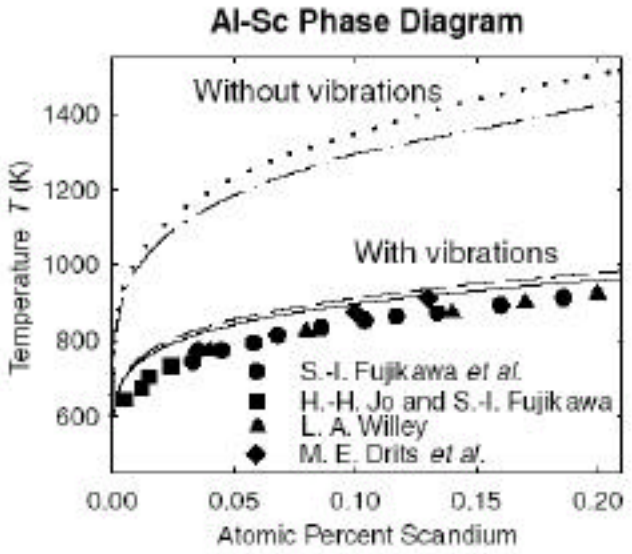

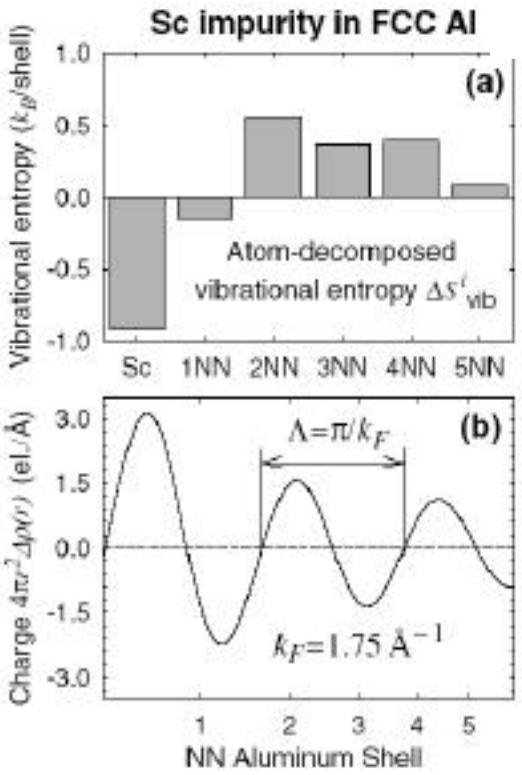

FIG. 2. Detailed analysis reveals that nearest-neighbor (NN) bond counting arguments are insufficient to explain the influence of vibrational effects on the Al-Sc phase diagram. Rather, we find that longer-ranged effects play a major role: Sc impurities induce perturbations in farther-neighbor Al shells that act to cancel out the vibrational entropy decrease from stiff NN Al-Sc bonds. Fig. 2(a) shows the atom-decomposed partial excess entropies for a Sc impurity in FCC Al. These entropies are defined in analogy with atom-decomposed partial phonon DOS:

$$\Delta S_{\rm vib}(i) = \sum_{\mathbf{q}\nu} |\mathbf{e}_i(\mathbf{q}\nu)|^2 S\left(\frac{\hbar\omega_{\mathbf{q}\nu}}{2k_BT}\right) - S_{\rm vib}^{\rm bulk}(i),$$

where $S(x) = x/\tanh(x) - \ln[2\sinh(x)]$ is the harmonic phonon mode entropy function, i labels atoms and $S_{\rm vib}^{\rm bulk}(i)$ is the vibrational entropy of the pure bulk constituent i. It is seen that the Sc impurity has the most negative $\Delta S_{\rm vib}(i)$, indicative of a strong and stiff Al-Sc bond. The nearest-neighbor Al shell shows a slightly negative $\Delta S_{\rm vib}(i)$, but the surrounding shells all contribute positive excess entropies, leading to a slightly positive net value of +0.36 k_B/atom. Two conceptually distinct effects contribute to the "softening" of farther-neighbor Al shells around a Sc impurity: (i) geometric volume change to accommodate the larger Sc atom, and (ii) electronic Friedel oscillations associated with the Sc impurity. We find a net charge transfer of 0.3 electrons to the Sc impurity and the surrounding twelve NN-Al atoms. This charge transfer is a consequence of the strong hybridization lowering the energy of the *p-d* bonding states between Al and Sc. In Fig. 2(b) we show the resulting Friedel oscillations around a Sc impurity. We find that the resulting changes in electronic charge density are of the same magnitude as those due to volume change, and they should therefore have comparable effects on the interatomic force constants.

Thermodynamic Properties of Al-Cu Alloys

C. Wolverton, X.-Y. Yan,** R. Vijayaraghavan,* and V. Ozolins*
**Ford Motor Company, MD3028/SRL, Dearborn, Michigan*
** University of Wisconsin, Madison, Wisconsin
****Sandia National Laboratories, California*

Publications:

C. Wolverton and V. Ozolins, "Entropically favored ordering: The metallurgy of Al_2Cu revisited." ***Physical Review Letters*** **86**, 5518 (2001).

C. Wolverton, X.-Y.Yan, R. Vijayaraghavan, and V. Ozolins, "Incorporating first-principles free energetics in computational thermodynamics approaches." To appear in *Acta Materialia* (2001).

Motivation:

Computational thermodynamic approaches have become a valuable tool in the calculation of complex, multicomponent phase equilibria often found in industrial alloys. These methods rely on databases of free energies, obtained from an optimization process involving experimental thermodynamic and phase diagram data. However, many phases of practical interest (e.g., metastable precipitate phases) are absent from computational thermodynamics databases, due to insufficient information to perform the optimization process. We demonstrate that first-principles, density functional calculations provide a means to obtain thermodynamic functions of phases absent from current databases. As an example to illustrate this hybrid first-principles and computational-thermodynamics approach, we consider the famous metastable Cu-containing precipitate phase, Al_2Cu-θ', often found in age-hardened aluminum alloys.

Accomplishment:

Many classes of industrial aluminum alloys are heat treated in practice to produce increased hardness due to precipitation microstructures. Cu is a commonly occurring solute element which can impart substantial hardening via the precipitates forming along the famous sequence of phase transformations in Al-Cu:

$$\text{Solid solution} \rightarrow \text{GP1, GP2 zones} \rightarrow Al_2Cu\ (\theta') \rightarrow Al_2Cu\ (\theta).$$

The metastable Al_2Cu-θ' phase is an important precipitate in this sequence and can lead to enhanced mechanical properties, but it is unfortunately absent from many computational thermodynamics databases. The reason for this absence is that the thermodynamics of this phase are not well characterized experimentally. In fact, even in the binary Al-Cu system the metastable θ' solvus is not well established.

The phase stability of Al_2Cu in the equilibrium θ and metastable θ' structures was previously investigated using first-principles calculations [see *Vibrational Stabilization of the* θ *phase in* Al_2Cu]. The surprising result from our work was that the energetic ground state of Al_2Cu is not θ, as might be expected from the generally accepted phase diagram. Instead, the calculated T=0 energy of the θ' phase is lower than that of θ. This apparent discrepancy between calculated T=0 energetics and the experimental observations at finite temperature can be reconciled by appealing

to the vibrational entropies of θ and θ'. A significant difference in vibrational entropies between the two phases serves to reverse the T=0 energetic tendency and stabilize θ at modest temperatures (i.e., above about 200 C). However, θ' is actually the stable ground state at low temperatures. From these first-principles calculations, one has the energetic and entropic contributions to the stability of θ vs. θ'. Combination of these contributions yields the free energy difference between θ and θ'': $\delta G(\theta'/\theta) = G(\theta')-G(\theta)$. We have used this quantity $\delta G(\theta'/\theta)$ in conjunction with available computational thermodynamics databases to calculate phase diagrams of binary and multicomponent Al-Cu alloys (see Fig. 1 below).

Significance:

Using first-principles methods, we have calculated free energies of θ and θ'' phases of Al_2Cu. We have found that the T=0 ground state of Al_2Cu is θ'' and not θ, as was thought before. We have also shown how to use the calculated first-principles free energy differences to supplement thermodynamic data and construct alloy phase diagrams.

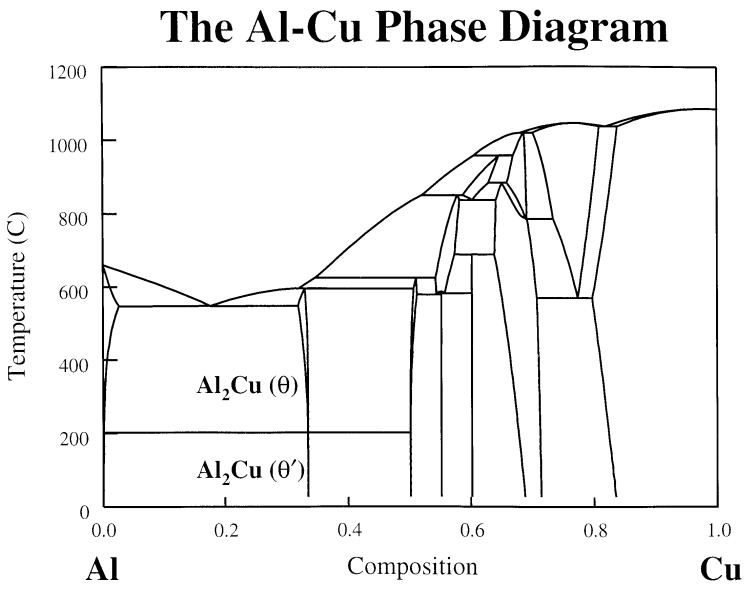

Fig. 1

Fig. 1 shows the equilibrium phase diagram of Al-Cu calculated using the WinPhaD program and database, combined with the first-principles calculated $\delta G(\theta'/\theta)$. As explained above, the first-principles results predict a surprising transition between the stability of θ and θ' around 200 C, and this transition is reflected in Fig. 1.

Thermodynamic Properties of Al-Sc Alloys

V. Ozolins* and M. Asta**
**Sandia National Laboratories, California*
*** Northwestern University, Evanston, Illinois*

Publications:

V. Ozolins and M. Asta, "Large vibrational effects upon calculated phase boundaries in Al-Sc." ***Physical Review Letters*** **86**, 448 (2001).

M. Asta and V. Ozolins, "Structural, vibrational and thermodynamic properties of Al-Sc alloys and intermetallic compounds." Physical Review B **64**, 094104 (2001).

M. Asta, V. Ozolins, and C. Woodward , "A First-Principles Approach to Modeling Alloy Phase Equilibria", JOM Vol. **53**, No. 9, 16 (2001).

Motivation:

Despite the growing interest in Al(Sc) alloys, uncertainties persist related to the Al-Sc phase diagram. For example, the crystal structure of the equiatomic AlSc phase remains uncertain, with both *B2* (CsCl prototype) and B_f (BCr prototype) structures having been reported in the literature. Recently, two assessments of the Al-Sc phase diagram have been published by Murray and Cacciamani *et al.* The optimized thermodynamic parameters obtained in these two assessments show significant differences, as do the calculated phase boundaries for near-equiatomic alloy compositions. At present, ternary additions to Al-Sc alloys are being investigated in the development of high specific-strength materials for potential applications at high homologous temperatures. As a basis for modeling phase stability in these multicomponent systems, an improved understanding of the binary Al-Sc phase diagram is desirable.

Accomplishment:

Previously a large effect of vibrational free energy upon calculated Sc solid solubility limits was found [see highlight *Large Vibrational Effects upon the Phase Diagram of Al-Sc*]. We extended our study of temperature-dependent structural and thermodynamic properties of solid-phase Al-Sc alloys and compounds based upon first-principles calculations of electronic free energies and ionic vibrational spectra. The contributions of non-configurational (electronic and vibrational) entropies to the free energies of solid-phase Al-Sc alloys and compounds are analyzed, and the accuracy of the approximations employed in these calculations is assessed. For each of the reported intermetallic compounds in this system, calculated formation enthalpies agree to within ten percent (0.05 eV/atom) of published calorimetric measurements. Large negative entropies of formation, equal to -0.77, -0.28 and -0.62 k_B/atom are calculated for cubic Al_3Sc, cubic AlSc and orthorhombic AlSc compounds, respectively, resulting primarily from the stiffening of nearest-neighbor Al-Sc bonds in the intermetallic phases relative to elemental Al and Sc. The net effects of non-configurational free energy contributions to the fcc portion of the Al-Sc phase diagram are 100 and 450 K decreases in calculated Al solvus phase boundary temperatures associated with electronic and vibrational entropy, respectively, at the maximum measured Sc solid-solubility limit. It is suggested that vibrational entropy may stabilize the orthorhombic B_f phase of AlSc just below the melting temperature.

Significance:

Our results point to a substantial effect of vibrational entropy upon calculated temperatures for phase boundaries between substitutional alloy phases with differing compositions. Further work on other Al-based alloy systems is currently being performed to assess the generality of our findings for Al-rich Al-Sc alloys. Preliminary results and previous analysis by Zener [*Thermodynamics in Physical Metallurgy*, edited by C. Zener (ASM, Cleveland OH, 1950), pp. 16-27] suggest that vibrational entropy leads to significant reductions in the temperature scales of calculated phase boundaries in a wide range of Al-based alloys. We also find that vibrational entropy may also tend to stabilize low-symmetry phases, such as orthorhombic B_f vs. cubic *B2* in AlSc, confirming earlier speculation about the generality of this phenomenon.

FIGURE:

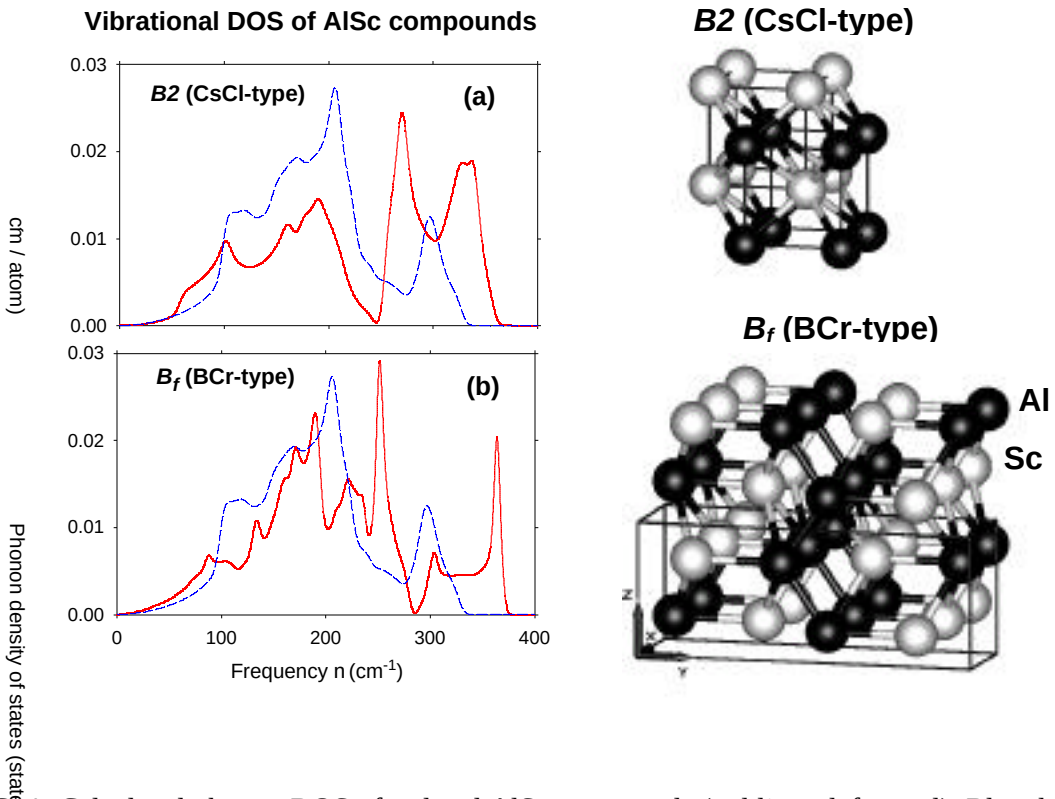

FIG. 1. Calculated phonon DOS of ordered AlSc compounds (red lines, left panel). Blue dashed line shows the composition-weighted phonon DOS of constituents. Due to less weight in the low-frequency region, both compounds exhibit negative entropies of formation. Crystal structure of the cubic *B2* and orthorhombic B_f structures are shown to the right. The orthorhombic B_f structure has a higher vibrational entropy and is predicted to be stable just below the melting point of AlSc.

Explanation of the INVAR Effect in FeNi Alloys

Mark van Schilfgaarde
Sandia National Laboratories, California

Publications:

M. van Schilfgaarde, I. A. Abrikosov, and B. Johanssön, **Nature 81**, 5149 (1999).

L. Dubrovinsky, N. Dubrovinskaia, I. A. Abrikosov, M. Vennström, F. Westman, S. Carlson, M. van Schilfgaarde, and B. Johanssön, **Physical Review Letters 86**, 4851 (2001).

Motivation:

The Fe-Ni alloy with a Ni concentration around 35 atomic % exhibits anomalously low, almost zero, thermal expansion over a considerable temperature range. This ``Invar'' effect has now been found in various ordered structures, random alloys or even in amorphous materials. Other physical properties of Invar systems, such as atomic volume, elastic modulus, heat capacity, magnetization, Curie (or Neel) temperature, also show anomalous behavior. It was realized early on that the explanation of the Invar effect is related to magnetism, but a detailed understanding was lacking.

Accomplishment:

Using a recently implemented non-collinear theory of magnetism within the local density approximation, we investigated thermodynamic properties for random fcc Fe-Ni Invar alloy. By a ``magnetic statics'' approach, we relaxed the noncollinear (canted) spin orientations of all the Fe and Ni spins, to obtain the ground state configuration. (This approach is analogous to a ``molecular statics'' widely used to obtain equilibrium nuclear positions. A ``spin dynamics'' analog of molecular dynamics is also possible.)

We found that the evolution of the magnetic structure even at zero temperature is characterized principally by a continuous transition from the ferromagnetic state at high volumes to a disordered noncollinear configuration at low volumes. There is an additional, comparable contribution to the net magnetization from the changes in the amplitudes of the local magnetic moments. The noncollinearity gives rise to an anomalous volume dependence of the binding energy curve, and explains the well-known peculiarities of Invar systems. Some subsequent experimental work verified a prediction that the same effect could be induced for different Fe concentrations under pressure. The left Figure shows the (continuous) transition from a collinear to a noncollinear configuration with decreasing volume. Panel (d) in the right figure shows that the Grüneisen parameter γ_{LT} passes through zero near the minimum-energy volume. The thermal expansion coefficient is approximately proportional to γ_{LT}.

Significance:

This work explained a long-standing problem of the origin of the Invar effect. It was also one the first practical applications of noncollinear density functional theory.

FIGURES:

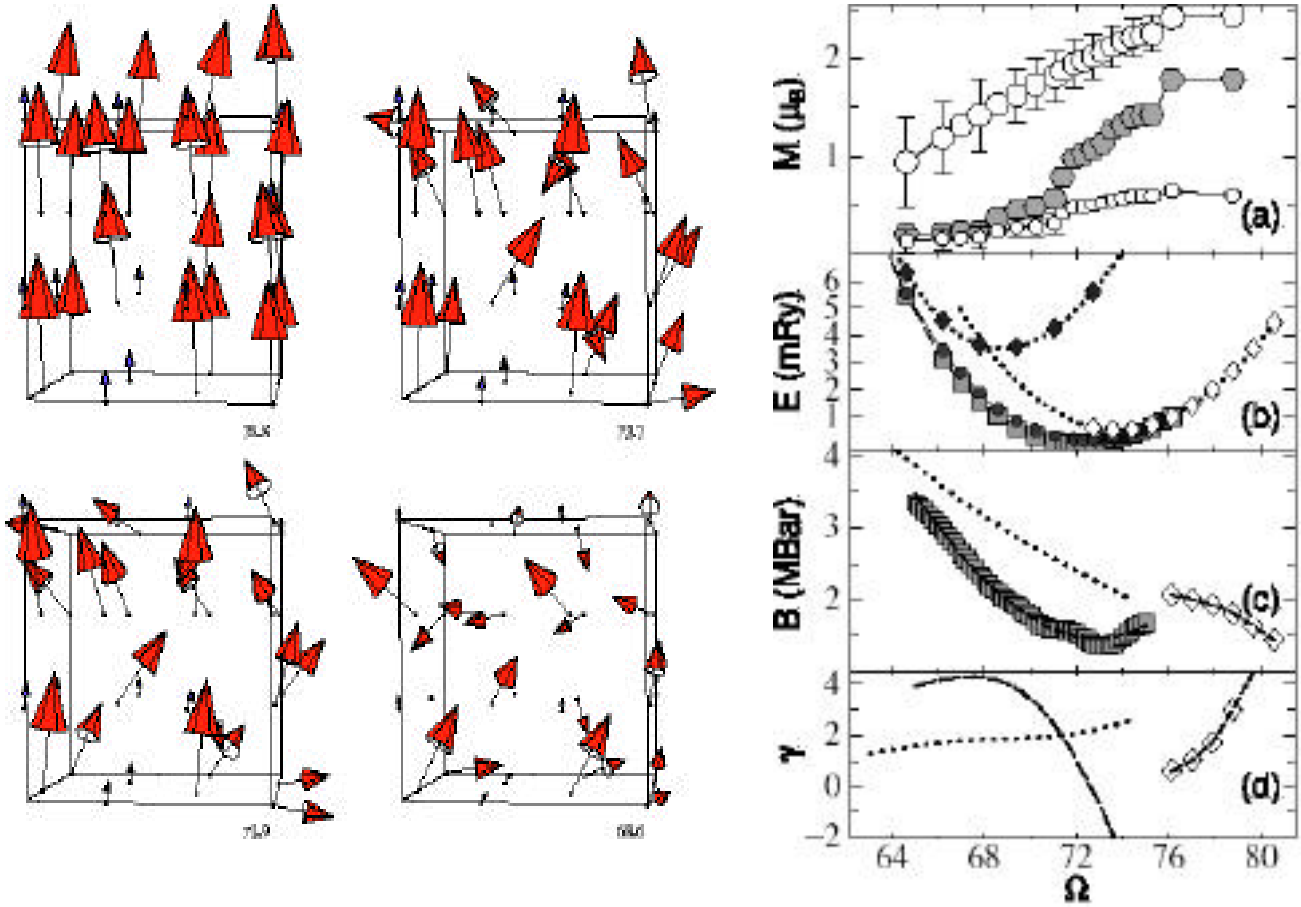

Left: Self-consistent magnetic spin configurations of the fcc Fe-Ni alloy at the four volumes 78.8, 73.7, 71.9, and 68.6 a.u.. Red and blue arrows show magnetic moments on Fe and Ni atoms, respectively. Arrow sizes reflect local moment amplitudes. The Ni spins are always approximately oriented along the average magnetization direction (vertical axis). The alloy is modelled by a supercell of 32 atoms with 21 Fe atoms and 11 Ni atoms randomly distributed

Right: volume-dependence of ground-state properties of the $Ni_{0.34}Fe_{0.66}$ alloy. Atomic volume is in atomic units. (a) Hexagons denote average magnetization per atom (in μ_B); large and small circles, the average absolute magnetic moments on the Fe and Ni sites, respectively. Error bars denote rms fluctuations in the moments. (b) Binding energy curve (in mRy). Dashed line, light squares: ground state energy from the noncollinear calculations. Dotted line, open and fill diamonds: ferromagnetic and nonmagnetic calculations, respectively, showing the classical high-spin to low-spin transition. Solid line, circles: collinear calculations. (c) Bulk modulus (MBar) obtained from differentiation of $E(\Omega)$. Diamonds and squares show the (ground state) ferromagnetic and noncollinear data, respectively. (d) Grüneisen constant γ_{LT}.

Short-Range Order in Surface Alloys

B. Sadigh, M. Asta, V. Ozolins, N. C. Bartelt, A. Schmid, and R. Q. Hwang
Sandia National Laboratories

Publication:

B. Sadigh, M. Asta, V. Ozolins, A. K. Schmid, N. C. Bartelt, A. A. Quong, and R. Q. Hwang, "Short-range order and phase stability of surface alloys: PdAu on Ru(0001)", **Physical Review Letters 83**, 1379 (1999).

Motivation:

In comparison with bulk alloys, several physical effects are unique to surface alloys due to the presence of substrate. Among these effects are surface stresses, elastic-dipole interactions, and surface –induced changes in chemical bonding. In order to determine their relative importance for specific thin-film alloy systems, detailed comparisons are needed between first-principles theoretical calculations and experimental measurements. We demonstrate how results of first-principles calculations and scanning-tunneling-microscopy (STM) imaging of alloy atomic structure can be used within the statistical-mechanical framework of lattice models to investigate quantitatively the energetic and thermodynamic properties of pseudomorphic surface alloys.

Accomplishment:

From scanning-tunneling microscopy (STM) images of *thermally equilibrated* samples, such as the one shown in Fig. 1(a), we have determined values of pair and triplet correlation functions for pseudomorphic Pd-rich alloys with a variety of Au compositions. In Fig. 2 we show the extracted Warren-Cowley short-range order (SRO) data for a $Pd_{0.61}Au_{0.39}$ surface alloy, obtained from an image containing 2609 atoms. The SRO data presented in Fig. 2 provides a basis for critically testing the predictions of the first-principles cluster expansion (CE) approach in its application to surface alloys. We used the CE method to calculate effective cluster (pair and triplet) interactions (ECIs) from first-principles total energies. These first-principles ECIs were used in Monte-Carlo simulations to compute SRO parameters for Pd-rich surface alloys. The image in Fig. 1(b) is a representative "snap-shot" from a Monte-Carlo simulation for $Pd_{0.72}Au_{0.28}$ at 570 K. The similarity between the chain features in Figs. 1(a) and 1(b) is apparent. To quantify the agreement between STM and the first-principles results for chemical SRO, we show in Fig. 2 first-principles-calculated SRO parameters for $Pd_{0.61}Au_{0.39}$ at 570 K. The agreement between the calculated and STM-measured results at the same composition is excellent.

Significance:

We have demonstrated how the energetic and thermodynamic properties of pseudomorphic thin-film alloys may be studied quantitatively within the framework of lattice models in combination with atomic-resolution STM imaging and first-principles total-energy calculations. For bulk alloys, diffuse-scattering measurements of SRO parameters continue to play an important role in the development of modern theories of bulk-alloy phase stability. However, these scattering measurements are significantly more difficult for surface alloys due to the extremely small scattering cross section associated with an ultrathin film. Therefore, the real-space analysis presented here, which is based upon STM measurements of thermally equilibrated samples, represents a useful alternative.

FIGURES

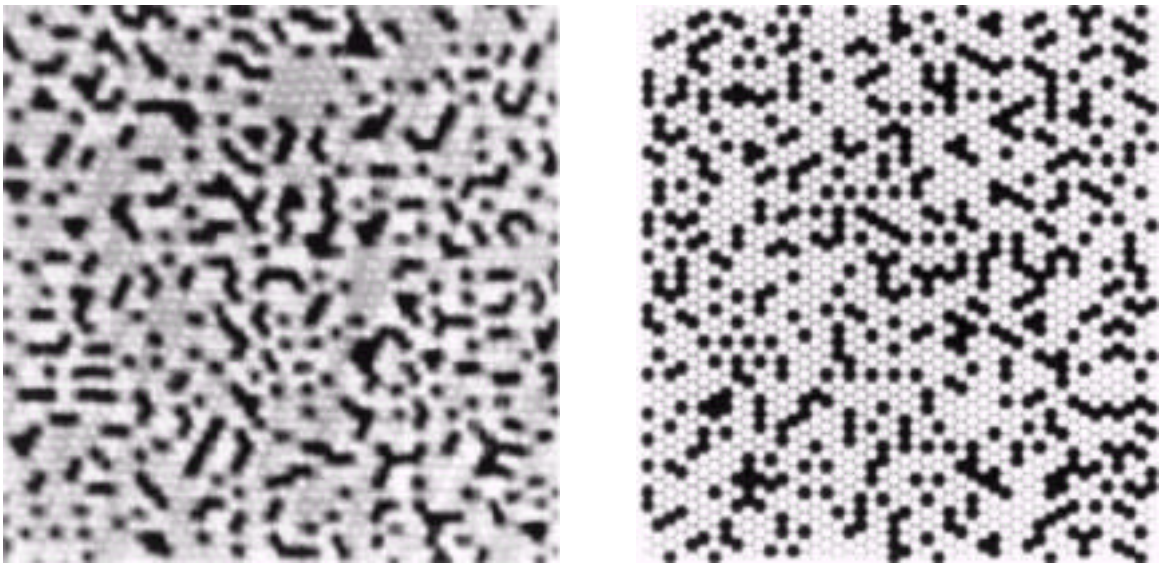

FIG. 1. STM-measured (a) and first-principles-calculated (b) structures for a $Pd_{0.72}Au_{0.28}$ alloy equilibrated at a temperature of T=573 K. The STM image is 12 nm by 12 nm in size, and in both (a) and (b) the black and gray atoms are Au and Pd, respectively.

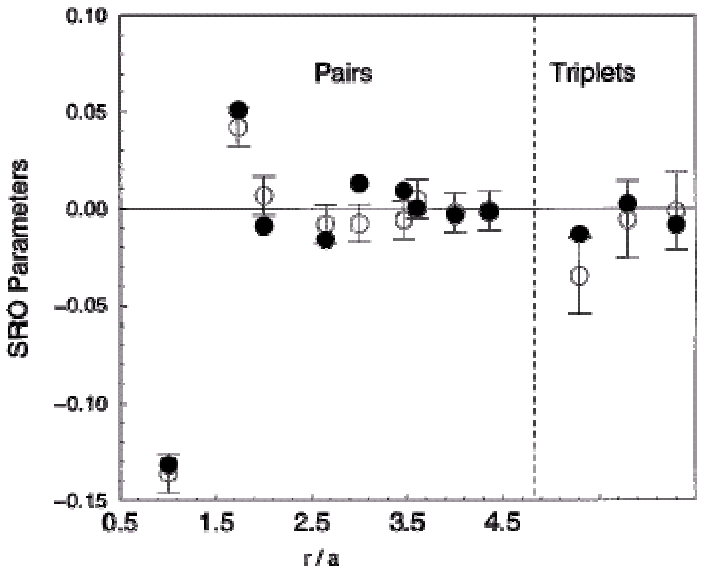

FIG. 2. STM-measured (open circles) and first-principles calculated (filled circles) SRO parameters for nine pair and three triplet clusters from a $Pd_{0.61}Au_{0.39}$ alloy equilibrated at *T=573* K. Results for the first two triplets correspond to the two symmetry-inequivalent equilateral NN triangles, while the third corresponds to the isosceles triangle made up of two nearest-neighbor and one second-neighbor pair.

The Role of Stress in Thin Film Alloys

G. E. Thayer, V. Ozolins, A. K. Schmid, N. C. Bartelt, and R. Q. Hwang
Sandia National Laboratories, California

Publication:

G. E. Thayer, V. Ozolins, A. K. Schmid, N. C. Bartelt, M. Asta, J. J. Hoyt, S. Chiang, and R. Q. Hwang, "Role of Stress in Thin Film Alloy Thermodynamics: Competition between Alloying and Dislocation Formation", **Physical Review Letters 86**, 660 (2001).

Motivation:

Surface stress due to crystalline lattice mismatch is well known to have a profound influence on the structure of surfaces and interfaces. Because interfacial structure is a dominant factor in the determination of new and interesting properties found in thin film structures and multilayer superstructures, a detailed understanding of the relation between surface stress and surface structure is important. Such an understanding requires an investigation in which theory and experiment are closely coupled.

Accomplishment:

We have investigated surface stress by using experimental measurements to make a detailed thermodynamic phase diagram of the structure of a surface alloy and comparing the data to well defined theoretical models. This study took advantage of the abilities of scanning tunneling microscopy (STM) to image surface structures with atomic resolution in order to observe the effects of surface stress in the structure of submonolayer Co-Ag films on Ru(0001). Co-Ag/Ru(0001) consists of two immiscible metals, Co and Ag, each with oppositely induced surface stress (due to lattice mismatch) when deposited on Ru, which causes a thin film alloy to form. When comparing the experimentally measured data with first-principles local-spin-density-approximation (LSDA) calculations, we discovered that multiple stress relief mechanisms resulted in a surface phase diagram that is different from the relatively simple progression of droplet and stripe phases predicted by well accepted continuum theories. The experimental data revealed a phase separation. Figure 1a shows a submonolayer $Co_{0.2}Ag_{0.8}$ alloy film, which was found to consist of two phases, a $Co_{0.6}Ag_{0.4}$ alloy phase and a pure dislocated Ag phase. This observation led to the improvement of our theoretical model that was then able to more closely match the experimental results. On the more local scale of 10Å, measured displacements of highly strained Co atoms found at the boundaries between Ag and Co (Figure 2) were compared to calculated data and found good agreement. This work was able to verify theoretical structural models that include short-range chemical forces and long-range elastic and point to some of their limitations.

Significance:

Using a combined experimental and theoretical approach, our investigation of Co-Ag/Ru(0001) has contributed to a more detailed understanding of the relation of surface stress to surface structure. The agreement between theory and experiment in this complicated system confirms the accuracy of our models and our ability to predict which interactions are involved on surfaces and their magnitudes. Since similar long-range and short-range interactions as well as stress relief

mechanisms will be features common to many surfaces and interfaces, these results in part contribute to understanding the factors that control the formation of new thin-film materials.

FIGURES

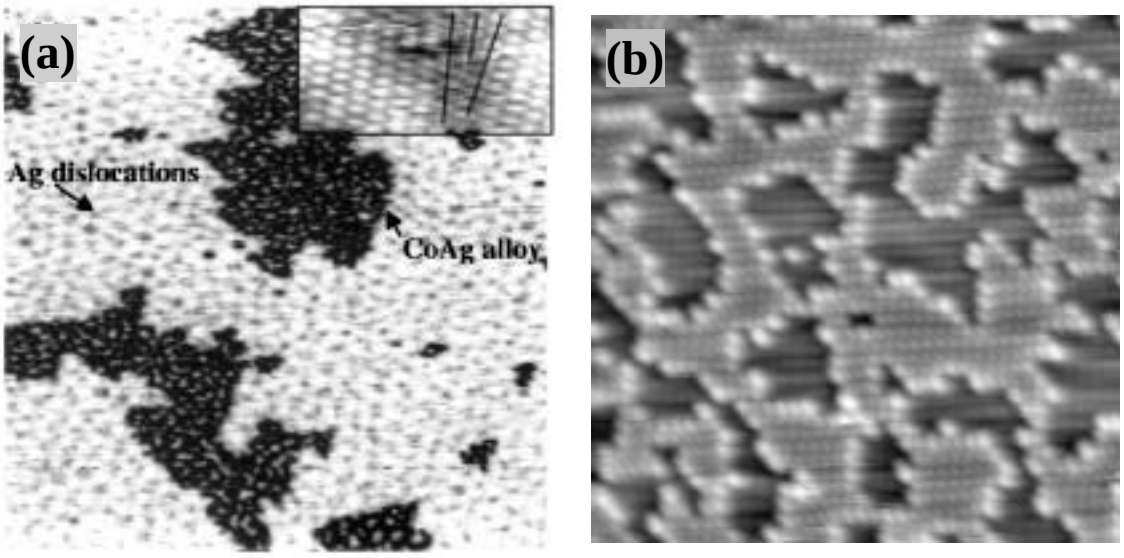

FIG. 1. Equilibrated Co-Ag films on Ru(0001). Phase segregation occurs for films with Ag composition greater than 40%. (a) 1000 Å x 1000 Å image (I_t = 0.50 nA, V_s = 0.58 V) of film with composition of 80% Ag. Inset shows atomic resolution of a single dislocation in the pure Ag phase, showing a missing row of atoms in the atomic lattice. (b) Atomic-resolution STM image of a thermally annealed Co-Ag surface alloy on Ru(0001), showing a disordered droplet structure. Ag atoms are dark and Co atoms are bright spots. Increased brightness of Co atoms near Co/Ag interfaces is due to atomic displacements, indicative of an efficient strain relief in the alloy phase.

FIG. 2. *Top*: Schematic representations of calculated configurations of Co-Ag: (a) reference state consisting of pseudomorphic phase-separated Co and Ag patches; (b) Co_mAg_m stripes; (c) hexagonally ordered droplet phases of Ag droplets in Co film. *Bottom*: Calculated surface energies at *T=0* K of Co-Ag stripes (black circles), droplets (gray circles), and 15/16 Ag dislocation on Ru(0001) (black square). The arrow points to the calculated composition for the onset of phase segregation. The solid line represents *T=0* K ground states. The inset shows formation energies of (100) stripe phases at *c=0.5*. The solid line in the inset represents a fit to the calculated values of $\Delta H(n)$ using the continuum expression introduced by Marchenko (1992) and Ng and Vanderbilt (1995):

$$\Delta H = \frac{I_C}{\Lambda} - \frac{I_E}{\Lambda}\ln\left(\frac{\Lambda}{a_{\mathrm{Ru}}}\right),$$

where $I_E > 0$, $I_C > 0$, and Λ is periodicity.

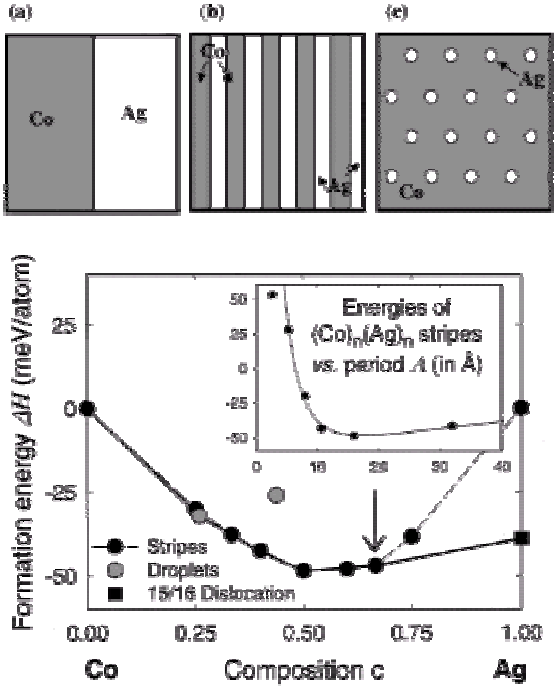

First-Principles Theory of Elastic Interactions in Surface Alloys

V. Ozolins,* M. Asta,** and J. J. Hoyt***
**Sandia National Laboratories, California*
*** Northwestern University, Evanston, Illinois*
****Sandia National Laboratories, New Mexico*

Publications:

V. Ozolins, M. Asta, and J. J. Hoyt, "Theory of Elastic Relaxations in Ultrathin Alloy Films," submitted to **Physical Review Letters** (2001).

M. Asta, V. Ozolins, and J. J. Hoyt, "The energetics of surface alloy formation: an embedded-atom-method, second-order-expansion study." *Modeling and Simulation in Materials Science and Engineering* **8**, 287 (2000).

Motivation:

Ordering and pattern formation on surfaces has emerged as a promising way of obtaining new materials with interesting and potentially useful properties. In particular, entirely new self-organized surface alloy phases have recently been created in the laboratory. Understanding why these new phases form, how they form, and how their behavior can be controlled is the main long-term goal of our work. Our goal is to develop a predictive theory of surface alloy thermodynamics that uses realistic surface-atom interactions obtained from first-principles electronic-structure calculations and configurational entropies obtained from Monte-Carlo simulations.

Accomplishment:

Chemical and elastic (both direct and substrate-mediated) interactions between surface atoms play equally important roles in stabilizing observed alloy structures. This property poses a formidable challenge since it requires a theory of surface alloy energetics that includes both positional and configurational degrees of freedom. We have adapted a theory originally developed for bulk alloys and modified it for the case of surface alloys. The Hamiltonian is given by:

$$H = \frac{1}{2}\sum_{\alpha\beta}\sum_{\mathbf{R},\mathbf{R}'} u_\alpha(\mathbf{R})\Phi_{\alpha\beta}(\mathbf{R}-\mathbf{R}')u_\beta(\mathbf{R}') + \sum_{\alpha}\sum_{\mathbf{R},\mathbf{R}'} S(\mathbf{R})K_\alpha(\mathbf{R}-\mathbf{R}')u_\alpha(\mathbf{R}') + \frac{1}{2}\sum_{\mathbf{R},\mathbf{R}'} J(\mathbf{R}-\mathbf{R}')S(\mathbf{R})S(\mathbf{R}'), \qquad (*)$$

where $u_\alpha(\mathbf{R})$ are atomic displacements, S($\mathbf{R}$) are pseudo-spin variables (+1 or –1) representing configurational degrees of freedom, and Φ, K, and J are interaction parameters that are obtained using first-principles calculations. We find that surface-atom relaxations tend to dominate for wavelengths of up to 20-30 lattice spacings, a fact that is not well represented in the conventional continuum-based approach used to treat elastic-dipole interactions in thin films. Configurational entropy is incorporated by subjecting the Hamiltonian (*) to standard Metropolis Monte Carlo simulations. We have applied the developed formalism to Co-Ag alloys on Ru(0001) surface and obtained very good agreement with experimental STM images (see below).

Significance:

We have developed a theory of surface alloy thermodynamics that is based upon first-principles energetics and statistical-mechanical treatment of configurational entropies. This theory has reliable predictive capabilities and can be applied to any ultrathin film surface alloy system. It is a step beyond the conventional continuum-based approach and points to serious limitations of the latter when applied to length scales of a few to tens of nanometers.

First-Principles Atomistic Structure of $Co_{0.60}Ag_{0.40}$ on Ru(0001)

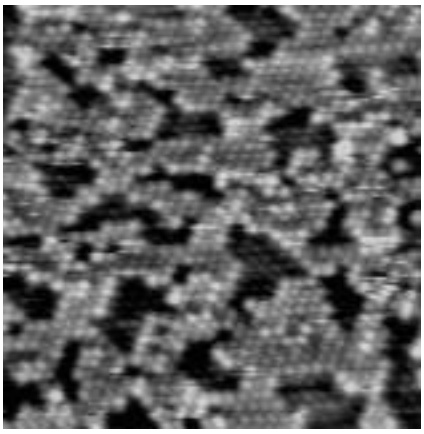

Fig. 1(a)

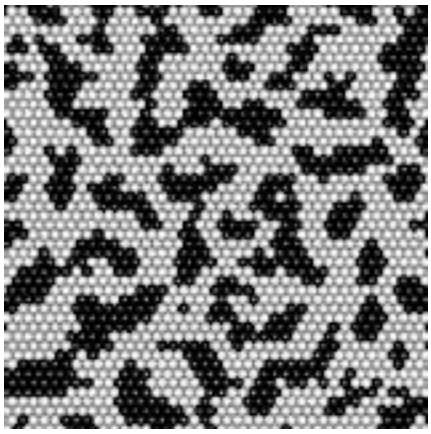

Fig. 1(b)

Figure 1(a) shows an atomic resolution STM image of a 60 at. % Co – 40 at. % Ag monolayer film on Ru(0001), exhibiting a disordered pattern of Ag islands (dark dots) in a Co matrix (gray dots). The sample was annealed at approximately 900 K [see G. Thayer, V. Ozolins, A. K. Schmid, N. C. Bartelt, M. Asta, J. J. Hoyt, S. Chiang, and R. Q. Hwang, "The role of stress in thin-film alloy thermodynamics: Competition between alloying and dislocation formation." ***Physical Review Letters*** **86**, 660 (2001)]. Figure 1(b) shows a snapshot from Monte Carlo simulations performed at T=900 K. Surface atom interactions were calculated theoretically using first-principles electronic-structure methods without any adjustable parameters. The disordered pattern of Ag droplets exhibits the same essential features as the experimental image to the left. Our calculations predict that below ~350 K the pattern orders into a regular array of Ag droplets or stripes, depending upon the composition of the surface alloy.

Ab Initio Molecular Dynamics Simulations of Liquid Ni-Al Alloys

M. Asta,* J. J. Hoyt,** V. Ozolins*** and M. van Schilfgaarde***
**Northwestern University, Evanston, Illinois*
***Sandia National Laboratories, New Mexico*
****Sandia National Laboratories, California*

Publication:

M. Asta, V. Ozolins, J. J. Hoyt, and M. van Schilfgaarde, "*Ab initio* molecular-dynamics study of highly nonideal structural and thermodynamic properties of liquid Ni-Al alloys", **Physical Review B Rapid Communications 64**, 020201 (2001).

Motivation:

Liquid Ni-Al alloys feature significant chemical short-range order, a large mismatch in atomic size, and highly non-ideal thermodynamic solution properties. These melts therefore share many features in common with structurally complex multicomponent liquids used in the processing of commercial alloys and in the production of bulk metallic glasses. The structural and thermodynamic properties of Ni-Al melts have been relatively well characterized, and this binary alloy serves as a non-trivial system for testing the accuracy of various simulation methods. To further understand the microscopic factors influencing non-ideal thermodynamic properties and interatomic diffusion in these alloys, we have for the first time undertaken *ab initio* molecular dynamics (AIMD) simulations of liquid Ni-Al.

Accomplishment:

In Fig. 1 we compare the calculated (solid line) and measured (symbols) Bhatia-Thornton structure factors for a $Ni_{20}Al_{80}$ liquid. The agreement between experiment and theory displayed in Fig. 1 is seen to be excellent for both the number-number and number-chemical correlation functions, $S_{NN}(q)$ and $S_{NC}(q)$. The AIMD simulations also reproduce the pronounced peak in the chemical-chemical structure factor (S_{CC}), indicative of a significant chemical short-range order (SRO) in the liquid. The chemical short-range order parameter α_{NiAl} was calculated to be –0.10, which compares very well with the value of α_{NiAl} =–0.09 derived from neutron-scattering measurements by Maret et al. [Phys. Rev. B **42**, 1598 (1990)]. The average length of Ni-Al bonds is found to be considerably shorter than either Ni-Ni or Al-Al bonds, in contrast with simple-minded hard-sphere considerations and indicative of strong chemical binding between atoms of unlike species. Strong interatomic bonding and chemical short-range order are found to affect the diffusion coefficient. AIMD calculated values of diffusion coefficients are much smaller than those obtained from classical EAM potentials, since the latter do not reproduce well the enhanced bonding and chemical SRO effect between unlike atoms. Finally, we have explained the apparent discrepancy between previously calculated values of excess entropy of formation of liquid Ni-Al alloys and experimental data. It has been attributed to entropy contributions associated with electronic excitations, which were not accounted for in any of the previous classical calculations. The magnitude of electronic excess entropy is calculated to be ΔS_{el}= -0.42 k_B/atom, which is 60% of the magnitude of ideal entropy of mixing at the same composition.

Significance:

Using *ab initio* molecular dynamics (AIMD), we were able to reproduce experimentally measured structural and thermodynamic data for liquid Ni-Al alloys. Compared with previous results obtained by classical EAM simulations, AIMD gives rise to a more highly ordered liquid

structure leading to lower calculated values for the diffusion coefficients. The AIMD simulations point to a significant non-configurational contribution to the excess entropy of formation for liquid Ni-Al alloys arising from electronic excitations. This contribution is very large (ΔS_{el}=*–0.42* k_B/atom) and explains previous disagreement between experimental data and classical EAM simulations.

FIGURES:

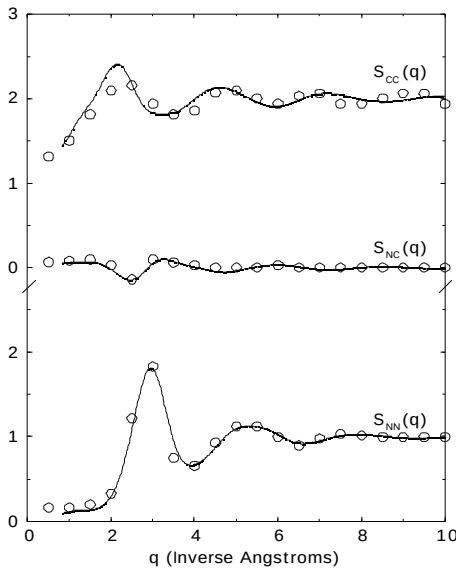

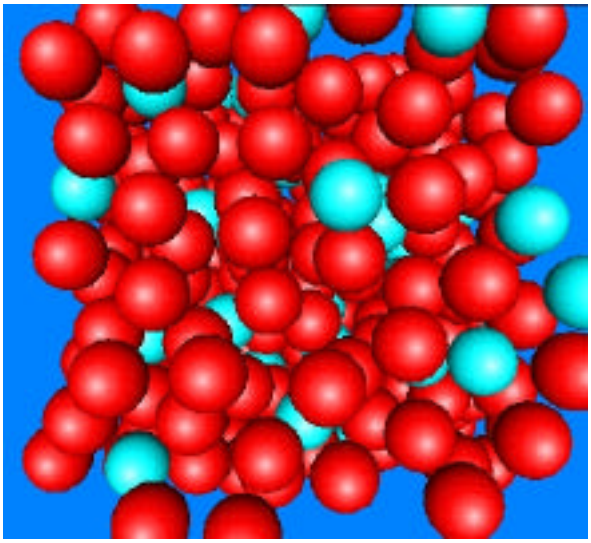

FIG. 1 **FIG. 2**

Figure 1 shows the calculated (solid line) and measured (open symbols) Bhatia-Thornton structure factors for a $Ni_{20}Al_{80}$. **Figure 2** shows a snapshot of atomic configuration of liquid $Ni_{0.20}Al_{0.80}$ at T=1300 K. It is apparent from this image that a significant degree of short-range order persists in the liquid, since almost all Ni atoms (cyan) are surrounded by nearest-neighbor Al atoms (red).

Computing the Anisotropy in the Solid-Liquid Interfacial Free Energy

J. J. Hoyt and M. Asta* [and] ***
**Sandia National Laboratories, California*
***Northwestern University, Evanston, Illinois*

Publication:

J. J. Hoyt, M. Asta, and A. Karma, "Method for Computing the Anisotropy of the Solid-Liquid Interfacial Free Energy", **Physical Review Letters 86**, 5530 (2001).

Motivation:

The formation of dendrites during the solidification of a liquid is an important process from both technological and scientific points of view. The mechanical integrity of a cast, brazed, or soldered alloy depends critically on the complex morphologies, which appear during solidification. In addition, dendrite formation represents a rather striking example of spontaneous pattern formation in a nonequilibrium system, a phenomenon studied extensively in many areas of physics, chemistry, and biology. Numerous studies over the last two decades have convincingly demonstrated that crystalline anisotropy plays a crucial role in dendritic solidification. Despite this progress, closure between theory and experiment has remained a major problem. A main obstacle is that the anisotropy of the solid-liquid interfacial energy is characteristically very weak for dendrite forming systems with low entropy of melting and atomically rough interfaces. Thus, the precise value of this key parameter controlling microstructural evolution has so far remained too difficult to compute or measure experimentally for metallic systems of practical relevance.

Accomplishment:

We circumvent the above difficulties by computing, instead of γ, the interfacial stiffness, γ''. These two anisotropies can always be related. Since stiffness is an order of magnitude more anisotropic than surface free energy γ itself, the stiffness anisotropy is much easier to compute accurately by MD simulations than the corresponding one for γ. To obtain the stiffness for a given orientation, we use the known fact that this quantity can be related to the spectrum of interfacial fluctuations in thermodynamic equilibrium. To see how this relationship comes about in the form appropriate for simulations, consider a thin slab that is infinite along the vertical y-axis, of width W along the x axis, and of thickness $b << W$ along the z axis. Furthermore, let $h(x)$ denote the height (y coordinate) of the fluctuating ribbonlike interface that separates the solid and liquid phases in this slab (see Fig. 1 below). For the slab, the ribbonlike interface shape can be written as a sum of Fourier modes: $h(x) = \sum_k A(k)\exp(ikx)$. A relation between the interface stiffness and the mean square amplitude $\left\langle |A(k)|^2 \right\rangle$ can then be obtained by noting that the mean energy in each Fourier mode must be equal to $k_B T_M$, where k_B is the Boltzmann constant and T_M is the equilibrium melting temperature. Using the expression for the interfacial energy integrated over the arclength along the ribbon, we obtain at once the desired relation between the interfacial stiffness and mean-square amplitude:

$$\left\langle |A(k)|^2 \right\rangle = \frac{k_B T_M}{bW(\gamma + \gamma'')k^2}.$$

The anisotropy can be easily seen in Fig. 3 that plots the reciprocal of the fluctuation spectra vs . k^2. According to the above equation, the slope of the lines in Fig. 2 is proportional to the stiffness for the stated orientation.

Significance:

In summary, the very small anisotropy in the solid-liquid interfacial free energy can be found by monitoring the fluctuations of the interface position during molecular dynamics simulations. The success of the technique stems from the fact that it is the stiffness, not the interfacial energy alone, that controls the fluctuation spectra and the stiffness can vary significantly as a function of orientation.

FIGURES:

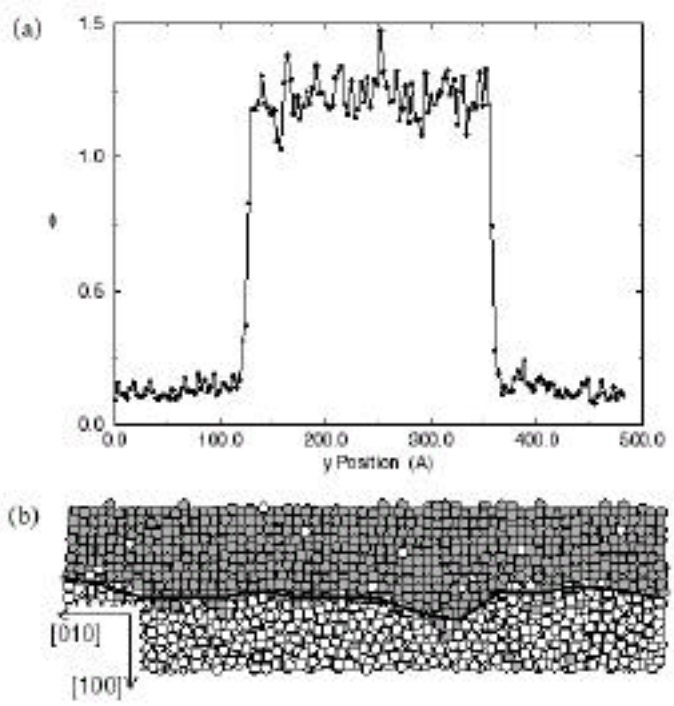

FIG. 1. Portion of the solid-liquid interface obtained from one snapshot of an MD simulation for the 100 [010] orientation (the thin direction, i.e., 001, points into the page). Atoms are shaded based on the value of the order parameter f defined in the paper. Superimposed as a thick line is the interface position corresponding to the *f=0.7* contour.

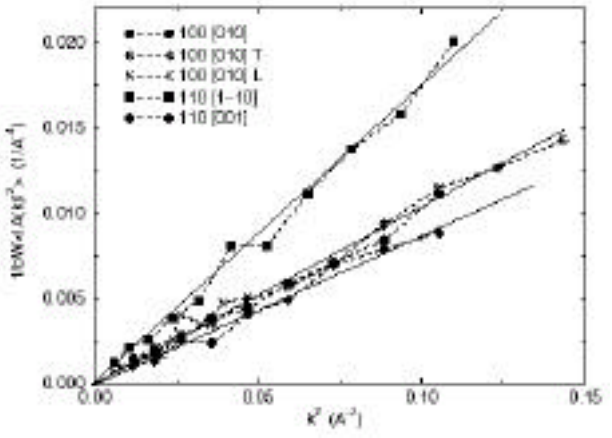

FIG. 2. $\left\langle |A(k)|^2 \right\rangle$ vs. k^2 for three crystal orientations. The slope of the lines is proportional to the solid-liquid interface stiffness and a clear anisotropy is observed. Also shown are results for different size simulation cells for the 100 interface (see the publication for more information).

Future Work

Surface ordering and self-assembly have emerged as promising approaches to tailor the properties of materials for use in microelectronics and micro-electro-mechanical systems.[58,59] Entirely new self-ordered surface alloy phases have recently been created in the laboratory [e.g., stripes in Co-Ag alloys on Mo(110)[60]]. *Understanding why these new phases form, how they form and how their behavior can be controlled will remain one of the main aspects of our program.* Emphasis will be placed on the development of atomistic and continuum models to study the equilibrium and non-equilibrium properties of surface and thin film self-organized alloy structures. Quantitative atomistic models of pattern formation in surface alloy films will be based upon first-principles electronic-structure calculations and rigorous statistical-mechanical treatment of thermodynamic free energies and driving forces for non-equilibrium processes. This work will continue to couple with experimental Ultra-High Vacuum (UHV) Scanning-Tunneling Microscopy (STM) and variable-temperature Low-Energy Electron Microscopy (LEEM) studies of both equilibrium film structure and time-dependent evolution. First-principles calculations will provide guidance in the selection of alloy systems for experimentation. Specific challenges include the following:

(i) Search for new materials that exhibit robust tendencies to self-organize at room temperatures and above. Extend the search to ternary systems, which should allow better fine-tuning of the balance between the competing effects of surface stresses and interfacial energies.

(ii) Explore effects of substrate structure and pre-patterning on the nucleation, growth and structure of the patterns. For instance, explore the effects of substrate anisotropy by studying ordered pattern formation on (100) and (110) surfaces of cubic crystals.

(iii) Study kinetics of pattern formation and kinetics of phase transitions between phases with different symmetry. For instance, study the transition from droplets to stripes with increasing area fraction of the minority phase.

Potential benefits of the proposed research are better understanding of how to achieve uniform size distribution of self-assembled nanostructures and how to control the size and periodicity of patterns. Uniform size distribution is important for various applications in catalysis and electronics, while the ability to tune the size of and separation between micro-domains is important, e.g., for magnetic materials.

Study of non-configurational entropies in bulk alloys will remain one of the key directions of future research. We will continue investigating other cases where vibrational entropies play an important role in the observed phase diagrams. Current work in progress at Sandia California indicates that solvus boundaries in numerous Al-based alloys (such as Al-Ti, Al-Ni, Al-Au, Al-Zr, and Al-Cu) are strongly influenced by vibrational entropy effects. These findings demonstrate the importance of vibrational entropy in a wide range of alloy systems.

One of the most important future tasks in the theory of substitutional alloys is developing methods for incorporating vibrational entropies in first-principles calculations of phase diagrams. Current work in progress at Sandia explores the idea of expanding the total energy of an alloy in terms of the atomic displacements $u_{i\alpha}$ and site-occupation variables S_i. This idea is an extension of

the classical Kanzaki-type Hamiltonian,[61,62] which expands the total energy to second order in configuration and displacement variables. Alloy Hamiltonian is formally written as:

$$H = E_0 + (1-2c)E_1 + \frac{1}{2}\sum_{i,j} J_{ij} S_i S_j + \frac{1}{2}\sum_{i,j} \Phi_{ij}^{\alpha\beta} u_{i\alpha} u_{j\beta} + \frac{1}{2}\sum_{i,j} K_{ij}^{\alpha} u_{i\alpha} S_j + \ldots, \qquad (1)$$

where higher-order multibody terms have been omitted for the sake of brevity. These higher-order will be included in our treatment since they describe the dependence of interatomic force constants on the local chemical environment, i.e., they describe the configurational dependence of phonon frequencies and vibrational entropies. Such a method would provide the additional benefit of accurately treating static displacements and elastic inhomogeneities. The crucial problem is how to determine the expansion coefficients in Eq. (1). Currently, the only first-principles method to do this is the computational alchemy approach developed by Baroni and collaborators.[63] Their method relies on a Taylor expansion in configuration variables S_i around a virtual-crystal reference state. This expansion may be poorly convergent (or even divergent) in alloy systems composed of species that are very different chemically. We plan to try a somewhat different approach. Linear response calculations will be used to obtain harmonic force constants for a set of ordered structures. Anharmonic third-order terms in atomic displacements can also be obtained using the so-called "2n+1" theorem of perturbation theory.[43,65] Kanzaki forces,[61] given by terms linear in atomic displacements $u_{i\alpha}$ will be calculated from standard supercell calculations. Results for different ordered structures will be used to obtain cross-terms between atomic displacements and occupation variables.

This approach has several advantages: (i) it can handle long-range elastic interactions, (ii) it uses Taylor expansion in variables that are "small" (atomic displacements), while a rapidly convergent cluster expansion is used for unrelaxed structural energies, (iii) it can treat large anharmonic displacements, and (iv) is suitable for use in Monte Carlo simulations.

A relatively new area of research in our program deals with effects of magnetic spin excitations in binary alloys. It is a logical extension of our on-going study of the effects of non-configurational entropies on the thermodynamic and structural properties of alloys. Furthermore, it will provide a link with programs at Sandia aimed at the understanding of the properties of magnetic materials (e.g., permalloys) used in micro-electro-mechanical devices, such as micro-motors and magnetic actuators. Traditionally magnetism has been studied using semiempirical methods based upon lattice spin models such as the famous Heisenberg exchange model.[66,67] These models contain various adjustable parameters that are difficult (and often practically impossible) to determine for alloy systems of practical interest. We intend to study the interplay between magnetism and atomic structure in alloys using first-principles methods of calculating magnetic exchange interactions and spin dynamics. Recent cutting-edge advances in computational methods[30–34,68–73] show the promise of revolutionizing future studies of magnetism since they provide reliable means of obtaining spin-spin interactions using a microscopic quantum-mechanical based approach. Our research efforts will focus on deeper understanding of the factors affecting local magnetic moments and on developing quantitative models that predict how magnetic moments and exchange interactions vary with changes in local atomic coordination and chemical composition.[74–78]

Finally, due to their technological importance in casting processes of commercial alloys, theoretical study of liquid alloys remains an important component of our research program. Liquid alloys are also interesting from a fundamental physical point of view, since they exhibit complex topological and chemical short-range-order phenomena that are seldom encountered in solids. We plan to continue applying first-principles molecular dynamics methods to calculate structural and thermodynamic properties of binary liquid alloys. In the nearest future we plan

specific applications to the technologically important Al-Cu and Al-Si alloy systems. Research in this area will involve close collaborations with Dr. C. Wolverton (Ford Motor Corp.), Prof. M. Asta (Northwestern University), and Dr. J. J. Hoyt (Sandia New Mexico).

References

1. F. Ducastelle, *Order and Phase Stability in Alloys* (North-Holland, New York, 1991).

2. D. de Fontaine, Solid State Physics **47**, 33 (1994).

3. A. Zunger, in *Statics and Dynamics of Alloy Phase Transformations*, edited by P. E. A. Turchi and A. Gonis, Vol. 319 of *NATO Advanced Study Institute*, Series B: Physics (Plenum, New York, 1994).

4. B. L. Gyorffy, D. D. Johnson, F. J. Pinski, D. M. Nicholson, and G. M. Stocks, in *Alloy Phase Stability*, edited by G. M. Stocks and A. Gonis (Kluwer, Dordrecht, 1998), p. 293.

5. *Materials Science and Technology: A Comprehensive Treatment*, edited by R. W. Cahn, P. Haasen, and E. J. Kramer, Vols. 1-15 (Weinheim, New York, 1994).

6. A recent review is given by A. van de Walle and G. Ceder in http://xxx.lanl.gov/abs/cond-mat/0106490, which is to appear in Rev. Mod. Phys. (2001).

7. L. Anthony, J. K. Okamoto, and B. Fultz, Phys. Rev. Lett. **70**, 1128 (1993).

8. B. Fultz, L. Anthony, L. J. Nagel, R. M. Nicklow, and S. Spooner, Phys. Rev. B **52**, 3315 (1995).

9. L. J. Nagel, L. Anthony, and B. Fultz, Philos. Mag. Lett. **72**, 421 (1995).

10. L. Anthony, L. J. Nagel, J. K. Okamoto, and B. Fultz, Phys. Rev. Lett. **73**, 3034 (1994).

11. V. Ozolins and M. Asta, Phys. Rev. Lett. **86**, 448 (2001).

12. A. van de Walle, G. Ceder, and U. V. Waghmare, Phys. Rev. Lett. **80**, 4911 (1998).

13. C. Wolverton and V. Ozolins, Phys. Rev. Lett. **86**, 5518 (2001).

14. *Magnetism*, edited by G. T. Rado and H. Suhl (Academic Press, New York, 1963).

15. *Magnetism and Metallurgy*, edited by A. E. Berkowitz and E. Kneller (Academic Press, New York, 1969).

16. P. Haasen, *Physical Metallurgy*, 3rd ed. (Cambridge University Press, Cambridge, UK, 1996).

17. For a recent review, see W. J. Boettinger, S. R. Coriell, A. L. Greer, A. Karma, W. Kurz, M. Rappaz, and R. Trivedi, Acta Mater. **48**, 43 (2000).

18. Within the BES Computational Materials Science Network, "Microstructural Evolution Based on Fundamental Interfacial Properties" project has a web-site with up-to-date information at http://cmpweb.ameslab.gov/cmsn/microevolproj.html.

19. R. Kikuchi, Phys. Rev. **81**, 998 (1951).

20. K. Binder (ed.), *Monte-Carlo Methods in Statistical Physics, in Topics in Current Physics Series*, Vol. 7. (Springer-Verlag, New York, 1986).

21. K. Binder (ed.), *Applications of the Monte-Carlo Method in Statistical Physics, in Topics in Current Physics Series*, Vol. 36 (Springer-Verlag, New York, 1986).

22. J. M. Sanchez, F. Ducastelle and D. Gratias, Physica **128A**, 334 (1984).

23. D. B. Laks, L. G. Ferreira, S. Froyen, and A. Zunger, Phys. Rev. B **46**, 12 587 (1992).

24. C. Wolverton, V. Ozolins, and A. Zunger, J. Phys.: Condensed Matter **12**, 2749 (2000).

25. S.-H. Wei and H. Krakauer, Phys. Rev. Lett. **55**, 1200 (1985).

26. D. J. Singh, *Planewaves, Pseudopotentials, and the LAPW Method* (Kluwer, Dordrecht, 1994).

27. O. K. Andersen, Phys. Rev. B **12**, 3060 (1975).

28. O. K. Andersen, O. Jepsen, and D. Glötzel, in *Highlights of Condensed-Matter Theory*, edited by F. Bassani, T. Fumi, and M. P. Tosi (North-Holland, New York, 1985), p. 59.

29. M. Methfessel, M. van Schilfgaarde, and R. A. Casali, "A Full-Potential LMTO Method based on smooth Hankel Functions", in *Electronic Structure and Physical Properties of Solids: The Uses of the LMTO Method*, Lecture Notes in Physics, Vol. **535**, edited by H. Dreysse (Springer-Verlag, Berlin, 2000).

30. A recent review is given by V. P. Antropov, B. N. Harmon, and A. N. Smirnov in J. Magn. Magn. Mater. **200**, 148 (1999).

31. V. P. Antropov, M. I. Katsnelson, M. van Schilfgaarde, and B. N. Harmon, Phys. Rev. Lett. **75**, 729 (1995).

32. M. van Schilfgaarde, V. P. Antropov, and B. N. Harmon, J. Appl. Phys. **79**, 4799 (1996).

33. A. Liechtenstein, M. I. Katsnelson, V. P. Antropov, and V. A. Gubanov, J. Magn. Magn. Mater. **67**, 65 (1987).

34. V. P. Antropov, M. I. Katsnelson, B. N. Harmon, M. van Schilfgaarde, and D. Kusnezov, Phys. Rev. B **54**, 1019 (1996).

35. G. Kresse and J. Hafner, Phys. Rev. B **47**, 558 (1993).

36. G. Kresse and J. Hafner, Phys. Rev. B **49**, 14 251 (1994).

37. G. Kresse and J. Furthmüller, Comput. Mater. Sci. **6**, 15 (1996).

38. G. Kresse and J. Furthmüller, Phys. Rev. B **54**, 11 169 (1996).

39. D. Vanderbilt, Phys. Rev. B **41**, 7892 (1990).

40. S. Baroni, P. Giannozzi, and A. Testa, Phys. Rev. Lett. **58**, 1861 (1987).

41. P. Giannozzi, S. de Gironcoli, P. Pavone, and S. Baroni, Phys. Rev. B **43**, 7231 (1991).

42. S. de Gironcoli, Phys. Rev. B **51**, 6773 (1995).

43. X. Gonze, Phys. Rev. B **55**, 10337 (1997); X. Gonze and C. Lee, Phys. Rev. B **55**, 10355 (1997).

44. V. Ozolins, *Ph.D. Theses*, Royal Institute of Technology, Sweden (1996).

45. D. R. Hamann, M. Schlüter, and C. Chiang, Phys. Rev. Lett. **43**, 1494 (1979); G. D. Bachelet, D. R. Hamann, and M. Schlüter, Phys. Rev. B. **26**, 4199 (1982).

46. A. M. Rappe, K. M. Rabe, E. Kaxiras, and J. D. Joannopoulos, Phys. Rev. B 41, 1227 (1990); N. Troullier and J. L. Martins, Phys. Rev. B **43**, 1993 (1991).

47. W. E. Pickett, Computer Phys. Rep. **9**, 115 (1989).

48. J. Ihm, A. Zunger, and M. L. Cohen, J. Phys. C **12**, 4409 (1979).

49. M. S. Daw and M. I. Baskes, Phys. Rev. B **29**, 6443 (1984).

50. M. S. Daw, S. M. Foiles, and M. I. Baskes, Mater. Sci. Rep. **9**, 251 (1993); S. M. Foiles, in *Equilibrium Structure and Properties of Surfaces and Interfaces*, edited by A. Gonis and G. M. Stocks, Vol. 300 of NATO Advanced Study Institute, Series B: Physics (Plenum, New York, 1992).

51. A. van de Walle and G. Ceder, Phys. Rev. B **61**, 5972 (2000).

52. V. Ozolins, C. Wolverton, and A. Zunger, Phys. Rev. B **58**, R5897 (1998).

53. M. E. Drits, L. S. Toropova, R. L. Gushchina, and S. G. Fedotov, J. Sov. Non Ferrous Met. Res. **12**, 83 (1984).

54. E. A. Marquis and D. N. Seidman, Acta Mater. **49**, 1909 (2001).

55. V. I. Marchenko, Sov. Phys. JETP Lett. **55**, 73 (1992).

56. D. Vanderbilt, Surf. Sci. **286**, L300 (1992); K. O. Ng and D. Vanderbilt, Phys. Rev. B **52**, 2177 (1995).

57. M. Maret, T. Pomme, A. Pasturel, and P. Chieux, Phys. Rev. B **42**, 1598 (1990).

58. G. A. Prinz, Science **282**, 1660 (1998).

59. F. J. Himpsel, J. E. Ortega, G. J. Mankey, and R. F. Willis, Adv. Phys. **47**, 511 (1998); F. J. Himpsel, A. Kirakosian, J. N. Crain, J.-L. Lin, and D. Y. Petrovykh, Solid State Commun. **117**, 149 (2000).

60. E. D. Tober, R. F. C. Farrow, R. F. Marks, G. Witte, K. Kalki, and D. D. Chambliss, Phys. Rev. Lett. **81**, 1897 (1998).

61. H. Kanzaki, J. Phys. Chem. Solids **2**, 24 and 107 (1957).

62. D. de Fontaine, Solid State Physics **34**, 73 (1979).

63. S. de Gironcoli, P. Giannozzi, and S. Baroni, Phys. Rev. Lett. **66**, 2116 (1991); M. Peressi and S. Baroni, Phys. Rev. B **49,** 7490 (1994); N. Marzari, S. de Gironcoli, and S. Baroni, Phys. Rev. Lett. **72**, 4001 (1994).

64. X. Gonze and J.-P. Vigneron, Phys. Rev. B **39**, 13120 (1989).

65. A. Debernardi and S. Baroni, Solid State Commun. **91,** 813 (1994); A. Debernardi, S. Baroni and E. Molinari, Phys. Rev. Lett. **75,** 1819 (1995).

66. T. Moriya, *Spin Fluctuations in Itinerant Electron Magnetism* (Springer-Verlag, Berlin, 1985).

67. K. Yosida, *Theory of Magnetism* (Springer-Verlag, Berlin, 1996).

68. S. Y. Savrasov, Phys. Rev. Lett. **81**, 2570 (1998).

69. Q. Niu and L. Kleinman, Phys. Rev. Lett. **80**, 2205 (1998).

70. R. Gebauer and S. Baroni, Phys. Rev. B **61**, R6459 (2000).

71. Q. Niu, X. Wang, L. Kleinman, W.-M. Liu, D. M. C. Nicholson, and G. M. Stocks, Phys. Rev. Lett. **83**, 207 (1999).

72. Y. Wang, G. M. Stocks, D. M. C. Nicholson, and W. A. Shelton, Computers and Mathematics with Applications **35**, 85 (1998).

73. B. Ujfalussy, X. D. Wang, D. M. C. Nicholson, W. A. Shelton, G. M. Stocks, Y. Wang, and B. L. Gyorffy, J. Appl. Phys. **85**, 4828 (1999).

74. Y. Wang, G. M. Stocks, D. M. C. Nicholson, W. A. Shelton, V. P. Antropov, and B. N. Harmon, J. Appl. Phys. **81**, 3873 (1997).

75. D. M. C. Nicholson, W. H. Butler, W. A. Shelton, Y. Wang, X. G. Zhang, G. M. Stocks, and J. M. MacLaren, J. Appl. Phys. **81**, 4023 (1997).

76. A. B. Oparin, D. M. C. Nicholson, X. G. Zhang, W. H. Butler, W. A. Shelton, G. M. Stocks, and Y. Wang, J. Appl. Phys. **85**, 4548 (1999).

77. T. C. Schultness, W. H. Butler, G. M. Stocks, S. Maat, and G. J. Mankey, J. Appl. Phys. **85**, 4842 (1999).

78. N. Y. Moghadam, G. M. Stocks, M. Kowalewski, and W. H. Butler, J. Appl. Phys. **89**, 6886 (2001).